

Ultraviolet Imaging of the $z=0.23$ Cluster Abell 2246

Robert H. Cornett¹, Ben Dorman^{2,3}, Eric P. Smith^{3,7},
 Michael A. Fanelli¹, William R. Oegerle^{6,7}, Ralph C. Bohlin⁴,
 Susan G. Neff³, Robert W. O’Connell², Morton S. Roberts⁵,
 Andrew M. Smith³, and Theodore P. Stecher³

ABSTRACT

We present deep ultraviolet observations of a field containing the cluster Abell 2246 ($z=0.225$) which provide far-ultraviolet (FUV) images of some of the faintest galaxies yet observed in that bandpass. Abell 2246 lies within the field of view of Ultraviolet Imaging Telescope (UIT) observations of the quasar HS1700+64, which accumulated over 7100 seconds of UIT FUV exposure time during the Astro-2 mission in March 1995. For objects found on both the FUV and ground-based V-band images, we obtain FUV ($\lambda \sim 1520\text{\AA}$) photometry and V-band photometry, as well as mid-UV ($\lambda \sim 2490\text{\AA}$) photometry from UIT Astro-1 observations and ground-based I-band photometry. We find five objects in the images which are probably galaxies at the distance of Abell 2246, with FUV magnitudes ($m(\text{FUV})$) between 18.6 and 19.6, and V magnitudes between 18.4 and 19.6. We find that their absolute FUV fluxes and colors imply strongly that they are luminous galaxies with significant current star formation, as well as some relatively recent, but not current, (>400 Myr ago) star formation. We interpret the colors of these five objects by comparing them with local objects, redshift-corrected template spectra and stellar population models, finding that they are plausibly matched by 10-Gyr-old population models with decaying star formation, with decay time constants in the range $3 \text{ Gyr} < \tau < 5 \text{ Gyr}$, with an additional color component from a single burst of moderate ($\sim 400\text{--}500$ Myr) age. From derived FUV luminosities we compute current star formation rates. We compare the UV properties of Abell 2246 with those of the Coma cluster, finding that Abell 2246 has significantly more recent star formation, consistent with the Butcher-Oemler phenomenon.

Subject headings: galaxies: clusters: individual (Abell 2246); ultraviolet emission

¹Raytheon STX Corporation, Code 681, Goddard Space Flight Center, Greenbelt MD 20771

²University of Virginia, Astronomy Department, P.O. Box 3818, Charlottesville, VA 22903

³Laboratory for Astronomy and Solar Physics, Code 680, Goddard Space Flight Center, Greenbelt MD 20771

⁴Space Telescope Science Institute, Homewood Campus, Baltimore MD 21218

⁵NRAO, 520 Edgemont Rd., Charlottesville, VA 22903-4575

⁶Department of Physics and Astronomy, Johns Hopkins University, Baltimore, MD 21218

⁷Visiting Astronomer, Kitt Peak National Observatory (KPNO), which is operated by Association of Universities for Research in Astronomy (AURA), Inc. under contract to the National Science Foundation

1. Introduction

UV images of local galaxies provide unique direct evidence about the morphology and quantitative nature of recent star formation, while UV images of objects at moderate redshifts (z up to ~ 0.3) extend the limits of direct knowledge of massive star formation back to more remote times. The darkness of the UV sky (O’Connell 1987) further enhances observational prospects in this waveband. However, deep UV images of such objects are rare because of the dearth of instruments with sufficient resolution and sensitivity. In this paper we discuss deep observations including photometry in the far UV ($\sim 1520\text{\AA}$; FUV) and mid UV ($\sim 2490\text{\AA}$; MUV) by the Ultraviolet Imaging Telescope (UIT) of a field which contains the cluster Abell 2246 (Abell 1958). Abell 2246 is only lightly obscured by Galactic foreground reddening ($E(B-V)=0.03$) but has nevertheless attracted few published observations. Cluster center, angular size, richness, and luminosity function data for Abell 2246 used here are from Hoessel, Gunn & Schneider 1983, Hoessel & Schneider 1985 and Struble & Rood 1987. With a distance of 900 Mpc and a look-back time of 1.2 Gyr (based on $z=0.225$, for $q_0 = 0.1$ and $H_0 = 75 \text{ km s}^{-1} \text{ Mpc}^{-1}$, adopted for this paper) galaxies in Abell 2246 are among the most distant and faintest yet observed in the far ultraviolet. They provide an important stepping stone to understanding observations of more distant objects in longer-wavelength bands.

2. Observations and Data Reduction

Figure 1 shows the UIT FUV image, the UIT MUV image, and the V-band image, co-aligned and with the same scale, produced as described in the rest of this section. North and East, and a 1' bar, are shown. Sources which are identified in this work as galaxies at the distance of Abell 2246 are outlined by circles and numbered as in Table 3. Other nonstellar sources found on both images including apparent foreground galaxies and the quasar HS1700+64, are outlined by squares.

2.1. Ultraviolet Images

The UIT images are approximately centered on the quasar HS1700+64, which was a high priority target for the Hopkins Ultraviolet Telescope (HUT) science program. It was observed during two orbits during December 1990 by the Astro-1 ultraviolet instruments, and seven orbits during March 1995 by Astro-2. The quasar, at $z=2.743$, was utilized as the background UV source for the measurement of Davidsen *et al.* 1996 of the HeII opacity

in the intergalactic medium. UIT and the Wisconsin Ultraviolet Photometer- Polarimeter Experiment (WUPPE; Nordsieck *et al.* 1991) were co-pointed with HUT for these observations.

UIT’s intensified film cameras obtained a total of 7 MUV exposures and 23 FUV exposures of a 40' diameter field surrounding the quasar, with exposure times ranging from 6 to 1947 seconds during the Astro missions. Astro-1 exposures of this field were made early in the mission. They have stellar full width at half-maximum (FWHM) $\sim 4''$, reflecting the image quality obtained before nominal pointing performance was achieved. However, the Astro-2 images are more typical of UIT data, having stellar PSFs with FWHM $\sim 3''$. During Astro 2, nine images were made through UIT’s broadest-band FUV filter, known as “B1”, which has effective wavelength for flat spectra 1521\AA , bandwidth 354\AA , and is blocked against Ly α skyglow. Five of these images with individual exposure times of more than ~ 1000 seconds are used in this study. No MUV images are available from the Astro-2 mission. Individual exposures used here are listed in Table 1. UIT film images are digitized, linearized, flat fielded, and absolutely calibrated. The calibration and reduction procedures, combined with UIT’s image intensifiers, which eliminate reciprocity failure, produce linear, high-precision photometric data with typical calibration uncertainties of order 15% for well-exposed sources. Details of UIT hardware, calibration, operations, and data reduction are in Stecher *et al.* 1992 and Stecher *et al.* 1997.

The FUV images listed in Table 1 were converted to intensity units using the FLIGHT22 calibration constants and processing (Stecher *et al.* 1997). The images were resampled in software to the astrometry of the single exposure UIT FUV2366, and added to create a “stacked” image with a total exposure time of 7152 seconds. Co-alignment of the individual exposures was based on the standard astrometric solutions derived for UIT images using HST guide stars as fiducials (Lasker *et al.* 1989). Typical positional errors resulting from this procedure, including image distortion residuals after correction (Greason *et al.* 1994), are $3-4''$, confirmed for these images by the measured FWHM of $\sim 3.5''$ for stars on the stacked image. Since the measured and expected astrometric alignment errors are only slightly larger than nominal single-exposure UIT values, no additional alignment procedures were performed. The central 1024×1024 pixel ($\sim 20'$) of the stacked image, which encloses both the cluster diameter of $18'$ and the field of view of our groundbased images, was extracted and used as the primary FUV dataset.

Quantitative experience with the photometric proper-

Fig. 1.— (a) The UIT FUV image. the field of view is $20'$ across. North, East, and a $1'$ bar, are noted. Sources identified here as galaxies at the distance of Abell 2246 are outlined by circles; other nonstellar sources found on both images including apparent foreground galaxies and the quasar HS1700+46 are outlined by squares. Source numbers refer to Table 3.

Fig. 1.— (b) The UIT MUV image, co-aligned and with the same scale as the FUV image; the field of view is $20'$ across. North, East, and a $1'$ bar, are noted. Sources identified here as galaxies at the distance of Abell 2246 are outlined by circles; other nonstellar sources found on both images including apparent foreground galaxies and the quasar HS1700+46 are outlined by squares. Source numbers refer to Table 3.

TABLE 1
UIT IMAGES

Image#	Field Center RA (2000.0) DEC	Exp. Time (sec)	Obs. Epoch (GMT)		Filter	Flight
FUV2015	17 00 45.1 +64 13 09.	974.	3/05/95	00:15	B1	Astro-2
FUV2074	17 00 45.1 +64 13 09.	1210.	3/06/95	00:34	B1	Astro-2
FUV2257	17 00 45.1 +64 13 09.	1460.	3/08/95	01:21	B1	Astro-2
FUV2260	17 00 45.1 +64 13 09.	1560.	3/08/95	02:50	B1	Astro-2
FUV2366	17 00 45.1 +64 13 09.	1946.	3/10/95	00:30	B1	Astro-2
NUV0176	17 00 36.7 +64 13 42.	745.	12/06/90	05:26	A1	Astro-1

ties of deep co-added photographic images is limited, so we have made a detailed study of the noise and calibration characteristics of the stacked image. The noise characteristics of single UIT images as determined from measurements of flat fields are well defined, and are quantified by the UIT “FFVAR” function in the UIT data reduction package (Stecher *et al.* 1997). A “variance image” was created by summing the variances computed by FFVAR for each pixel of each of the exposures used to create the stacked image. The stacked image’s noise characteristics were also computed directly by measuring pixel-to-pixel variations on the image itself. We compare the results of these noise determinations to similar quantities derived from a single deep exposure (FUV2366) in the “stack”. Table 2 illustrates these results. The square root of the exposure time ratio between the stacked image and the single image is 1.91. The measured noise at sky levels (“ σ_{SKY} ”) obtained by measuring pixel-to-pixel variations on the images themselves, is 2.06 times larger for the single image than for the stacked image. In comparison the ratio of sigmas (“ σ_{FFVAR} ”) computed from the FFVAR function,

$$\sigma_{FFVAR}(FUV2366)/\sigma_{FFVAR}(STACK) = 1.65.$$

The low measured sky noise, smaller than the exposure time ratio predicts and smaller than the calculated value, is probably due to smoothing induced by misalignments among the component exposures of the stacked image, over both fixed-pattern noise and faint sources. The real improvement in signal-to-noise achieved by stacking is smaller than the exposure time ratio predicts, since the photon statistics implied by scaling with exposure time are a best-case limit for photographic film detection and are appropriate only for well-exposed UIT pixels.

The absolute calibration of the stacked image was verified by comparing the flux measured in the image for the quasar HS1700+64 with that obtained simultaneously by HUT (Davidsen *et al.* 1996). The stacked image’s FUV flux for the quasar, measured in an aperture with diameter 20” and sky-subtracted, agrees within 6.5% with the HUT sky-subtracted spectrum (kindly supplied by G. Kriss) made through a similar aperture, integrated over the UIT B1 bandpass. This difference is typical of comparisons of UIT’s absolute calibration with other instruments; when verified in this way, we estimate UIT’s absolute calibration uncertainty to be $\sim 10\%$.

The mid-UV (MUV) image used in this study, from a single exposure of 745 seconds, was converted to intensity units using the FLIGHT15 calibration constants and processing developed for Astro 1 (Stecher *et al.* 1997) and re-sampled in software to the astrometry of image FUV2366. The resolution of this image as determined by the stellar PSF FWHM is $\sim 4''$ compared to the usual MUV image value of $2.7''$ for images with nominal pointing quality. Because the bandwidth of the MUV “A1” filter is 3.24 times that of the “B1” filter, and because of a known, quantified decrease in UIT sensitivity for long exposures during the Astro-2 mission, the expected sensitivity limit of the MUV image is only 0.4 magnitudes brighter than that of the stacked FUV image. However, the MUV image is “confusion limited” at magnitude $m(MUV) \sim 20.0$ due to the high density of noise spikes and the high frequency of spurious sources against the sky background. For this reason we do not accept the presence of a source on the MUV image as sufficient confirmation for detection, and include as sources only objects that appear on both the FUV and the V-band images.

TABLE 2
NOISE CHARACTERISTICS OF STACKED IMAGES

	FUV2366	Stacked Image
Exp. Time	1946.	7152.
$\sqrt{\text{Exp. time ratio}}$	—	1.91
σ_{SKY} (erg (cm ² Å s) ⁻¹)	3.3×10^{-18}	1.6×10^{-18}
σ_{FFVAR} (erg (cm ² Å s) ⁻¹)	5.1×10^{-18}	3.1×10^{-18}

No independent check of MUV absolute calibration for this image is available because no simultaneous MUV observations of the quasar HS1700+64 were made and no suitable IUE comparison sources are present in the UIT field of view. For such cases we estimate the uncertainty in the UIT absolute calibration to be $\sim 15\%$.

2.2. Optical-band Images

The optical-band images, originally obtained in the course of a program to investigate star formation in Abell clusters, were made with the KPNO 0.9m telescope on 1994 July 9 using the the 2048×2048 T2KA CCD, which has $0.68''$ pixels. The $23'$ field was centered at RA= $17^h 01^m 14.7^s$, DEC= $64^\circ 11'45.1''$ (J2000.0).

The standard UVBRI filter set was used to make broad-band images for photometry of cluster members; those with blue colors ($B-V < 0.8$) were selected as candidates for later WIYN/HYDRA spectroscopy. Poor seeing caused the stellar FWHM in the Abell 2246 exposures to be $2.6''$.

V- and I-band images are used in this work. The total exposure times for V-band and I-band images were each 2700 sec, with three 900-sec exposures combined to produce the final images. Data were calibrated by comparing data from images of M92 made during the same night with published magnitudes.

2.3. Source Detection and Photometry

The V-band image was used as a guide to locating galaxies in the field. First, non-stellar sources were found by eye on the logarithmically stretched V-band image. The locations of V-band objects on the the stacked FUV image were then searched by eye for sources within $\sim 4''$. Apparent FUV sources were confirmed and located by centroiding (that is, by computing the flux-weighted mean posi-

tion). Data are in Table 3, which includes positions, the distance (“Dist.”) from the nominal cluster center in arcminutes, magnitudes in the UIT FUV ($\lambda 1520$) and MUV ($\lambda 2490$) filters, and V and I magnitudes. Seven FUV sources (Nos. 1-7 in Table 3) corresponding to V-band sources were located using this procedure.

In addition, the automated extended-source detection and photometry package FOCAS (Valdes 1982) was run on the stacked image for comparison. FOCAS detected a total of 79 sources including stellar ones, but did not find sources 4,6, and 7 in Table 3, probably because they are diffuse. Subsequent inspection of the V-band image at the locations of FOCAS-found FUV sources confirmed 6 additional objects, numbered 8-13 in Table 3. Of these only source 8 appears non-stellar on the V-band image. All 13 sources on the stacked FUV image were also found by eye on the MUV image. Observed positions, magnitudes, and V-band appearance are given in the Table.

Aperture photometry was performed on the images as follows; slightly different techniques were used for the UV and optical bands. For the UV images, a center pixel for each source was chosen, either by centroiding the source or, when centroiding failed, using the peak pixel. Aperture photometry in a circular aperture with radius $3.4''$ (11 kpc at $z=0.225$) was performed centered at that pixel location. A local sky was subtracted, measured using the mean sky value in an annulus between radii of 22 and $33''$, after removal of outliers. (A mean sky value is used for UIT images because the nonlinear density-to-intensity conversion produces a skewed pixel value histogram which does not lend itself to mode or median statistical techniques.) The variance in the UIT fluxes was computed conventionally, treating the source pixels as individual measurements of different quantities, and the sky pixels as individual and independent measurements of a single quantity. Because

Fig. 1.— (c) The CTIO V image. the field of view is $20'$ across. North, East, and a $1'$ bar, are noted. Sources identified here as galaxies at the distance of Abell 2246 are outlined by circles; other nonstellar sources found on both images including apparent foreground galaxies and the quasar HS1700+46 are outlined by squares. Source numbers refer to Table 3.

TABLE 3
PHOTOMETRIC RESULTS ^a

Source #	Position RA (2000.0) DEC	Dist. ^b '	m(FUV) ^c mag	m(MUV) ^d mag	V ^e mag	I ^e mag	Notes ^f
1	17 02 08.6 +64 12 20.1	9.2	18.27±0.14	18.44±0.16	16.66	16.53	FG
2	17 01 00.5 +64 12 8.9	1.9	17.12±0.10	17.75±0.16	16.32	16.86	QSO
3	17 01 06.3 +64 14 5.0	2.8	18.85±0.21	19.04±0.17	18.41	18.73	E,S?
4	17 00 38.0 +64 13 46.9	1.2	19.35±0.33	19.51±0.20	18.38	18.37	FG
5	17 00 31.4 +64 14 42.6	2.4	18.61±0.17	19.11±0.17	18.61	18.97	E,S?
6	17 00 35.3 +64 15 21.1	2.8	19.62±0.43	19.86±0.23	18.97	18.99	E?
7	16 59 31.8 +64 11 20.1	8.0	18.99±0.23	19.45±0.19	18.67	18.96	E?
8	17 00 54.6 +64 04 3.5	8.7	19.43±0.34	19.90±0.25	19.63	19.79	E,S?
9	17 00 34.4 +64 04 45.7	8.0	19.72±0.48	19.08±0.17	15.98	16.41	*
10	17 00 31.7 +64 07 58.5	4.9	19.72±0.47	21.67±1.03	21.11	19.34	?
11	17 01 15.0 +64 17 0.6	5.5	19.34±0.31	20.10±0.27	19.00	18.11	*
12	17 00 38.7 +64 22 14.9	9.5	21.17±1.26	21.19±0.69	17.76	18.17	?
13	17 00 24.1 +64 03 19.4	9.6	19.71±0.47	23.09±3.94	19.63	17.86	*

^aNot corrected for foreground extinction

^bFrom nominal cluster center

^c1520 Å

^d2490 Å

^eUncertainty, dominated by standard star measurements, is 0.05 mag

^fFrom appearance on V-band image: FG=foreground galaxy; QSO=quasar; E=elliptical galaxy; S=spiral galaxy; *=star

photographic noise increases rapidly at small signals, sky measurement dominates the UV flux uncertainties. Therefore the random uncertainties in flux units for all sources in each UV band are approximately equal ($\sim 1.6 \times 10^{-17}$ erg (cm²Å s)⁻¹ in the FUV, corresponding to a source of $m(\text{FUV}) \sim 20.9$; and $\sim 7 \times 10^{-18}$ erg (cm²Å s)⁻¹ in the MUV corresponding to $m(\text{MUV}) \sim 21.8$). Uncertainties shown in Table 3 for the FUV and MUV magnitudes include random error computed in this way as well as absolute calibration uncertainties of 10% in the FUV and 15% in the MUV. For the optical-band images standard FOCAS aperture photometry procedures, including sky determination and subtraction, were used, with aperture sizes matched to those used in the UV. Photometric uncertainties in the optical-band data are dominated by the reference-star uncertainties, which we estimate at 5%.

3. Discussion

Abell 2246, centered at RA=17^h 00^m 44^s, DEC=64° 12.7' (J2000.0) with a diameter of 18', is completely contained within the extracted UIT sub-images centered on HS1700+64 as well as within the optical-band images. The objects 3,5,6,7, and 8 in Table 3 are likely member galaxies of Abell 2246 from several lines of argument. First, they appear non-stellar on the V- and I-band images, with sizes corresponding to linear extents of a few tens of kpc at $z=0.225$. Second, their foreground- and redshift-corrected (FUV-V) colors, in the range -0.36 to +0.49, are similar to those of well-known local, bright star-forming galaxies (see Figure 3 and Table 4, where derived FUV absolute magnitudes, UV colors, and star formation rates for these five galaxies are presented.). Third, their UV luminosities, if they are at the Abell 2246 distance, are approximately those of nearby UV-luminous galaxies.

Redshifts are necessary to confirm certainly that these five objects are not foreground galaxies. However two points very much strengthen the case for this. From the UIT data compiled by Fanelli *et al.* 1998, the vast majority of field candidates, with “normal” FUV fluxes ($M(\text{FUV}) > -18.5$) have significantly lower FUV surface brightnesses. Thus they cannot be placed in front of Abell 2246 so that both their diameters and magnitudes scale to the observed values. Nearly all elliptical galaxies (e.g. all in Virgo) as well as a large fraction of spirals (e.g. M81 and NGC 2903) are eliminated; high-luminosity objects which are allowed by this criterion must have $DM > 37.5$, within a factor of 3 of the distance of Abell 2246.

The strongest argument against foreground interlopers, however, is the rarity of field galaxies, based on the

very low frequency of *any* extragalactic FUV sources seen in this (1520Å) bandpass in the complete UIT Astro-2 dataset. This bandpass excludes light longward of 1800Å and is therefore not sensitive to stellar populations characterized by stars cooler than $T_{eff}=9000\text{K}$, as discussed below. Astro-2/UIT imaged 42 40-arcmin diameter extragalactic fields (that is, with $|b| > \sim 30^\circ$ and excluding large foreground objects such as Galactic clusters and Local Group galaxies) with exposure times longer than 1000 seconds, with a conservative limiting magnitude of $m(\text{FUV}) \sim 18.5$. This image set was searched at the positions of all known extragalactic objects from the catalogs of de Vaucouleurs *et al.* 1991, Paturel *et al.* 1989, Huchra *et al.* 1995, Nilson 1973, Veron-Cetty & Veron 1996, and the IRAS Point Source Catalog. After excluding each field’s principal target and 9 known Coma Cluster members, a total of 16 objects were found and identified. Therefore, the rate of detection of serendipitous but catalogued FUV sources is about 0.4 objects per 40 arcmin UIT field, or 0.1 objects per (20-arcmin) Abell 2246 field, to $m(\text{FUV})=18.5$. We use the mid-UV ($\sim 2000\text{\AA}$) luminosity function of Milliard *et al.* 1992 for background galaxies to scale by 1.2 magnitudes to our Abell 2246 field limit of $m(\text{FUV})=19.7$, obtaining 0.6 possible foreground or background object per Abell 2246-sized field, compared with five detected objects. Hence, the extreme rarity of serendipitous extragalactic FUV sources strongly supports identifying these objects as members of Abell 2246.

Figure 2 shows $\sim 1'$ subimages of the five sources in Table 4 identified here as galaxies at the distance of Abell 2246. The subimages, in the V, MUV and FUV bands respectively, have the the same orientation as Figure 1. The objects are clearly not point sources, although the amount of morphological information available from the images is limited.

Assuming a distance modulus of 39.8 mag (based on $z=0.225$; Struble & Rood 1987), we determine absolute FUV magnitudes (corrected for Galactic foreground extinction using $E(B-V)=0.03$ and the extinction law of Cardelli, Clayton, and Mathis 1988) in the range from -21.4 to -20.4 (Table 4). A (FUV-V), FUV color magnitude diagram for Abell 2246 galaxies and well-known local objects (Fanelli *et al.* 1998) is shown in Figure 3. In this and subsequent plots all observations have been corrected for Galactic foreground extinction. (Note that while the color error bars from Table 4 would be a large fraction of the plot’s color scale, the plot’s entire range covers only the colors of stellar spectral types B9 through early A, showing the leverage of the FUV bandpass in this spectral range.) The effect of K corrections is shown by arrows,

Fig. 2.— Subimages of the five sources 3,5,6,7 and 8 in Table 3 which we identify in this work as galaxies at the distance of Abell 2246, in the FUV (left) MUV (center) and V (right) bands respectively. Orientation is the same as in 1, and the angular scale is shown by a $10''$ bar. The distance and surface brightnesses of the galaxies limit morphological information in the images, although the objects are clearly not point sources.

TABLE 4
INTRINSIC FUV PROPERTIES OF ABELL 2246 GALAXIES ^a

Source #	M(FUV)	FUV-V	MUV-V	SFR $M_{\odot}\text{yr}^{-1}$
3	-21.20	0.28	0.49	2.9
5	-21.44	-0.16	0.36	3.7
6	-20.43	0.49	0.75	1.4
7	-21.06	0.16	0.64	2.6
8	-20.62	-0.36	0.13	1.7

^aAfter correction for Galactic foreground ($E(B-V)=0.03$) and $D.M.=39.8$

which display the changes in (FUV-V) color and FUV magnitude obtained by redshifting representative galaxy and starburst spectra. To compute these vectors we have used the template spectra of Kinney *et al.* 1996, which provide spectral information across the wavelength range from 1200 to 10000 Å. (In this paper we use “K correction” to mean a transformation to rest-frame quantities, and “redshift correction” to mean its inverse, a transformation to observed quantities). The vectors shown are the redshift corrections ($z=0.225$) of the Sc galaxy template, the mean redshift correction of the Sb and Sc galaxy templates, and the mean redshift correction of starburst templates of all internal reddenings, of Kinney *et al.* 1996. (These redshift correction vectors are intended to show displacements only; their locations are arbitrary). The observed cluster galaxies evidently have color-magnitude loci which lie within the range of luminous blue local objects. However, K corrections are significant. For example, if all the Abell 2246 objects are Sc galaxies, some are intrinsically brighter in the FUV than M101, a luminosity class I Sc.

Figure 4 compares the (MUV-V, FUV-V) colors of Abell 2246 galaxies with the integrated colors of local galaxies (labelled). The Abell 2246 objects, observed at $z=0.225$, have slightly redder FUV-V colors than the rest-frame values of the bluest star-forming systems that are plotted here. For comparison, the colors of individual annuli from M33 and M74 (*cf* Figure 7 in Cornett *et al.* 1994) form a linear distribution that runs approximately from the locations of NGC1404 to NGC2993 on this plot, with colors from the outermost regions of these galaxies near those

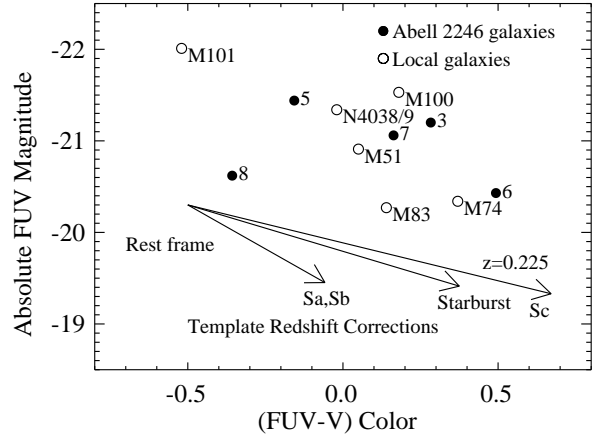


Fig. 3.— A (FUV-V), V color absolute-magnitude diagram for Abell 2246 (filled circles) and well-known local objects (open circles, labeled). All observations have been corrected for Galactic foreground extinction. (Note that while the color error bars from Table 4 are a large fraction of the plot’s color scale, the plot’s entire range covers only the colors of stellar spectral types B9 through early A, showing the leverage of the FUV bandpass in this spectral range.) Without redshift corrections, the observed cluster galaxies have FUV colors and magnitudes which lie within the range covered by local objects. Redshift-correction vectors for template spectra of Sa and Sb galaxies (averaged), starbursts with a range of internal reddenings (averaged), and Sc galaxies are also shown; appropriate redshift corrections are evidently significant. The vectors are intended to show displacements only; their locations are arbitrary.

of NGC2993.

Figure 5 compares the (MUV-V, FUV-V) colors with data from the individual template galaxy and population spectra of Kinney *et al.* 1996, also shown as averages in Figure 3. (This Figure has error bars appropriate for Figures 4, 5, and 6). The template spectra are constructed from composites of ground-based and IUE spectra of individual galaxies made through apertures matched to the $\sim 10 \times 20''$ large IUE aperture. The colors plotted, from upper left to lower right, range from those of composite starburst galaxies with small $(E(B-V) < 0.1)$ to large $(E(B-V) \sim 0.5)$ internal reddening as measured by Balmer decrements, through galaxies of increasingly earlier (“Sc, Sb, Sa, S0, E”) type, to those of a bulge (“B”) population. Each template color is plotted as viewed in its rest frame (diamonds) and redshifted to $z=0.225$ (crosses). The template starburst and Sc colors as well as the observed galaxy colors are in good agreement with bluer examples from the same bands from disk annuli in the local spiral galaxies M74, M81, and M33 (Cornett *et al.* 1994).

We have also computed and redshifted the spectral energy distributions (SEDs) of selected stellar population models of Bruzual & Charlot 1993, shown in Figure 6. The lower pair of curves shows single-burst star-formation models (that is, which have no star formation after age ~ 0), having solar metallicity, an initial mass function (IMF) slope of -1.35 , and a range of ages. The evolutionary tracks of those models as viewed in their rest frame (diamonds) and with a redshift of $z=0.225$ (crosses) are shown, along with the colors of the observed cluster galaxies (filled circles). The model starbursts shown range from age 0.1 Gyr (upper left of the diagram) to 0.6 Gyr (lower right) in ~ 0.1 Gyr increments. Evidently the observed galaxies are ~ 1 mag bluer in (FUV-V) than redshifted single-burst models of the observed (MUV-V).

The upper pair of curves in Figure 6 shows the effect of longer-term evolution. Those curves display colors from a decaying continuous star-formation model of Bruzual & Charlot 1993, with a star formation decay rate time constant of $\tau=1$ Gyr, with age increasing from ~ 0 to 6 Gyr from upper left to lower right. This model, which contains both younger and older stars than single-burst models, produces (FUV-V) colors which are up to ~ 0.7 mag bluer than observed galaxies in Abell 2246, for the observed (MUV-V).

The models’ behavior in the color-color plane of Figure 6 may be explained as follows. For any reasonable IMF, the UIT FUV bandpass is dominated by the hottest main sequence stars. Redshifting the spectrum to $z=0.225$ accentuates this, shifting the effective bandpass of obser-

vation to shorter λ (1060-1460Å). Therefore the evolution of FUV flux, and (FUV-V) color, tracks changes in the total flux of the hottest main sequence stars. This is borne out in the “Decaying SFR” models: both the rest-frame and redshifted colors are evenly spaced with time in (FUV-V), showing a simple power-law decrease. This behavior reflects the exponential fall-off in numbers of the hottest stars with decaying star formation rate. The color decay is nearly linear in this log-log plot because radiation at shorter (K-corrected) wavelengths selects the hottest stars even more stringently than the uncorrected bandpass. Single-burst models become redder in (FUV-V) more rapidly than “Decaying SFR” models, because the upper end of the decaying main sequence becomes cooler and redder, not just less populous. The bend in the evolutionary curve of the single-burst models, which strongly resembles the locus of the colors of stellar atmospheres of a wide range of temperatures in this plane, is caused by the rapid fall-off of sensitivity of the FUV bandpass to cooler stars: at about $T_{\text{eff}} = 9000\text{K}$, the peak of those stars’ UV continuum moves longward of the FUV long-wavelength cutoff at $\sim 1800\text{Å}$. Stars much cooler than this contribute significantly to MUV flux, but not to FUV. The location of the observed objects at significantly bluer (FUV-V) than redshifted single-burst models implies the existence of star formation more recent than the burst’s age ($\sim 400\text{-}500$ Myr) in the observed galaxies.

The effects of redshift in Figure 6 are of special interest. For SEDs with current star formation and therefore a significant hot-star component, correction to $z=0.225$ moves the models to bluer colors in both (FUV-V) and (MUV-V), *upward* along the aging line. In such SEDs both the FUV and MUV flux increase relative to V with redshift as more of the rising part of the hot-star continuum is shifted into those bandpasses. This is opposite to the cases of the templates (Figure 5) and single-burst models, whose SEDs lack any contributions from the hottest stars.

The filled diamond symbols represent the rest-frame colors of models of 10-Gyr-old stellar populations with different SFR decay times (Cornett *et al.* 1994). They simulate a galaxy with a long history of star formation as well as strong current star formation, and may be used to constrain the time dependence of that star formation. Since these model SEDs contain important contribution from the hottest stars, redshift corrections will move their colors upward and to the left along their locus, shortening their apparent SF decay timescale. After this redshift correction, models consistent with Abell 2246 galaxy colors have star formation decay timescales of $3\text{ Gyr} < \tau < 5\text{ Gyr}$. The models are still ~ 0.5 mag too blue in (FUV-V);

however, adding single-burst models with late A stars as their brightest component will add V and MUV flux, but not FUV.

From the above discussion it is evident that a combination of past star formation, as represented by single-burst models, and current star formation, as included in the models of Bruzual & Charlot 1993, can produce the colors observed in Abell 2246. The 10-Gyr-old decaying-SFR population with $3 \text{ Gyr} < \tau < 5 \text{ Gyr}$ overestimates the proportion of current star formation, with resulting (FUV–V) colors that are too blue. Conversely, a single-burst population of age $\sim 400\text{--}500 \text{ Myr}$ is too red in (FUV–V), and implies that more recent star formation is required. We conclude that the observed Abell 2246 galaxies a) are UV-luminous, with some as bright in the FUV as M101, depending on the assumed spectrum and resulting redshift correction. b) have FUV–V colors that show clear evidence of the flux of relatively young ($< 100 \text{ Myr}$) stellar populations, and are undergoing significant current star formation; but c) like observed late-type spiral galaxies, probably require flux contributed by stars of a range (up to $> 400 \text{ Myr}$) of ages.

This mixture of populations is like that of the objects known as “E+A” or “poststarburst” galaxies identified by Dressler & Gunn 1981. Spectra of these objects are thought to show evidence of recent ($10^8\text{--}10^9 \text{ yr}$ preceding the rest-frame epoch), vigorous star formation which has since decreased dramatically. Liu & Green 1996 model optical-band spectrophotometry of eight such objects having $0.088 < z < 0.545$. Their models are constructed from a linear combination of two spectral components: a composite spectrum of either an E/S0 or Sbc galaxy template; and a starburst with an age in the range 10^8 to $2 \times 10^9 \text{ yr}$. Figures 5 and 6 show that it is likely that such a combination would produce UV colors like those of Abell 2246 galaxies as well. The red colors of all templates except the “Sc” example in Figure 5, compared to those of Abell 2246 galaxies, make it clear that a late-type underlying galaxy is required to model these FUV-bright objects.

The current FUV flux, a direct tracer of massive stars and therefore of recent star formation, permits estimating rates for formation of massive ($M > 5 M_\odot$) stars. Following Lequeux *et al.* 1981, we use stellar evolutionary models of Schaller *et al.* 1992, Schaerer *et al.* 1993, and Charbonnel *et al.* 1993 with the stellar atmosphere models of Kurucz. For comparison with Donas *et al.* 1990, our selected IMF is a two-component power law with a break at $M = 1.8 M_\odot$, with low-mass slope -0.6 and high-mass slope -2.5 . For simplicity we use a model with constant star formation, which has constant UV flux after 100 Myr

(Landsman, personal communication), so our integration times are chosen to be 300 Myr . This model allows us to approximate the star formation rate as a function of the FUV (1520\AA) luminosity as

$$SFR = \frac{L_{1520}}{4.46 \times 10^{39}} M_\odot \text{yr}^{-1}$$

This expression gives good agreement with other models having similar assumptions (*cf* Donas *et al.* 1990), in view of the uncertainties present in the approach. Star formation rates computed from this expression for Abell 2246 galaxies, ranging from 1.4 to $2.9 M_\odot \text{yr}^{-1}$, are given in Table 4. These values are lower limits for actual SFRs, since extinction will decrease the apparent L_{1520} values. The expected redshift correction for *current* star formation rates at $z=0.225$, as discussed below, is small.

Only a few nearby clusters of galaxies have been observed in any ultraviolet bandpass. Donas *et al.* 1991 and Donas *et al.* 1995 discuss $\sim 20''$ resolution images of a local benchmark, the Coma cluster, in a bandpass $\sim 150\text{\AA}$ wide centered at $\sim 2000\text{\AA}$, deriving a UV luminosity function including 254 galaxies. It is particularly straightforward to compare their observations with our MUV photometry of Abell 2246 galaxies, because the central wavelengths of the bandpasses in the clusters’ rest frames are nearly equal (1955\AA for Donas *et al.* 1991 observations of Coma vs 2033\AA for our MUV bandpass at Abell 2246) and both observations contained the entire clusters in their respective fields of view.

Assuming a distance modulus of 34.8 for Coma based on $z = 0.023$ (Thompson & Gregory 1980) we use the MUV luminosity function of Donas *et al.* 1991 to determine that Coma, at the distance of Abell 2246, would have ~ 12 UIT-detected galaxies given our limit of $m(\text{MUV}) \sim 19.9$. A small richness correction derived by scaling the absolute numbers of Abell 2246 galaxies and Coma galaxies modifies the number of Coma galaxies seen at the Abell 2246 distance to be $\sim 13\text{--}14$. This result is consistent with the MUV data for Abell 2246: while only 5 Abell 2246 galaxies are *uniquely* detected and identified because of the confusion due to multiple sources, many more are apparent in the image. Large numbers of detectable MUV sources are present in the UIT MUV image of Abell 2246 because the MUV bandpass, sensitive to stars as late in spectral type as F, detects bright elliptical galaxies as well as those with current star formation.

The number of FUV-bright galaxies in Abell 2246 is apparently higher than in the Coma Cluster, however. We may make that comparison using UIT Astro-2 FUV observations (1900 sec exposure time; detection limit $m(\text{FUV}) \sim 19.0$)

of a field containing the central $\sim 40'$ of the Coma cluster. The two brightest galaxies in the UIT field, NGC4858 and IC4040, have UIT-determined $m(\text{FUV})$ of 14.65 and 14.70, respectively. Both are spirals and IRAS sources, and are among the six brightest Coma galaxies in the MUV according to Donas *et al.* 1991. These two galaxies, at the distance of Abell 2246, would have $m(\text{FUV})$ of 19.65 and 19.70 respectively—slightly fainter than the faintest observed Abell 2246 galaxy. Taking into account the redshift correction to $z=0.225$ depends critically on stellar content. SEDs with significant young stellar population (*e.g.* upper curves in Figure 6) have essentially unchanged FUV flux ($|\Delta m(\text{FUV})| < 0.1$), while SEDs without the youngest stars become 0.8-1.0 magnitudes fainter at $z=0.225$. In either case, these two galaxies would be fainter than detected Abell 2246 galaxies.

We also compare estimates derived from MUV observations of the entire Coma cluster by Donas *et al.* 1991. Coma's MUV luminosity function shows only 1 galaxy, NGC 4848 at $m(\text{MUV})=13.8$, brighter than $m(\text{MUV})=14.6$. (NGC 4848 and other brighter members were outside the UIT Coma field of view). If we assume NGC4848 to have FUV flux and colors indicating significant recent star formation, then $(\text{FUV}-\text{MUV}) \sim -0.5$, and the FUV redshift correction is small, resulting in $m(\text{FUV})=18.2-18.4$, 0.3 mag brighter than any Abell 2246 galaxy. If we assume NGC4848 to have the colors of normal spiral galaxies, then $(\text{FUV}-\text{MUV}) \sim 0.0$, and NGC4848 at Coma would have, after redshift correction, $m(\text{FUV}) = 19.6-19.8$, approximately equal to the faintest observed Abell 2246 galaxy. A FUV measurement of NGC4848 would resolve this ambiguity; in either case NGC4848 is the only Coma galaxy that is possibly brighter in the FUV, and all others are certainly fainter, than Abell 2246 galaxies. It is noteworthy that the radial distribution within the cluster of identified Abell 2246 FUV sources is similar to Coma's distribution of MUV sources (Donas *et al.* 1995), with 3 of 5 Abell 2246 galaxies at a radius ~ 0.33 of the Abell radius (though the statistics are inadequate).

The rarity of FUV-bright Coma cluster galaxies is evidence that Abell 2246 has undergone significantly more recent star formation than Coma (which nonetheless shows, in its MUV characteristics, evidence of star formation within the past 1 Gyr; *cf* Donas *et al.* 1995). This comparison is relevant to the Butcher-Oemler effect (Butcher & Oemler 1978; Butcher & Oemler 1984) wherein clusters are found to contain fractions of blue galaxies (as determined by restframe $(B-V)$) which increase with redshift. The FUV-bright galaxies in Abell 2246 directly show high

rates of star formation ~ 1.2 Gyr ago at $z=0.225$, which are not present to the same extent at more recent times and smaller redshifts in Coma. FUV data uniquely confirm the nature and scope of this star formation; additional FUV imaging of clusters such as Abell 2246 with higher sensitivity and finer resolution will be vital in bridging the gap between the local neighborhood and the distant universe.

We gratefully acknowledge the contributions made by the many people involved in the Astro-2 mission. We thank Joan Hollis and Joel Offenberg for careful and creative image processing and programming help.

Funding for the UIT project has been through the Space-lab Office at NASA under project number 440-51. RWO gratefully acknowledges NASA support of portions of this research through grants NAG5-700 and NAGW-2596 to the University of Virginia.

REFERENCES

- Abell, G. O., 1958, ApJS 3, 211.
- Bruzual, A. G. & Charlot, S. 1993, ApJ 405, 538.
- Butcher, H. & Oemler, A. 1978, ApJ 219, 18.
- Butcher, H. & Oemler, A. 1984, ApJ 285, 426.
- Cardelli, J. A., Clayton, G. C., and Mathis, J. S. 1988 ApJ329, L33.
- Charbonnel, C., Meynet, G., Maeder, A., Schaller, G., & Schaerer, D. 1993, A&AS 101, 415.
- Cornett, R. H., O'Connell, R. W., Greason, M. R., Offenberg, J. D., Angione, R. J., Bohlin, R. C., Cheng, K. P., Roberts, M. S., Smith, A. M. Smith, E. P., Talbert, F. D., and Stecher, T. P. 1994, ApJ 426, 553.
- Davidson, A. F., Kriss, G. A., & Zheng, W. 1996, Nature 380, 47.
- Donas, J., Buat, V., Milliard, B., & Laget, M. 1990, A&A, 235, 60.
- Donas, J., Milliard, B., & Laget, M. 1991, A&A, 252, 487.
- Donas, J., Milliard, B., & Laget, M. 1995, A&A, 303, 661.
- Dressler, A. & Gunn, J. E. 1981, ApJ270, 7.
- Fanelli, M. A. *et al.* 1998 in preparation.
- Greason, M. R., Offenberg, J. D., Cornett, R. H., Hill, R. S., & Stecher, T. P. 1994 PASP 106, 1151.

- Hoessel, J. G., Gunn, J. P., & Schneider, D. P. 1983, *ApJ* 264, 337.
- Hoessel, J. G. & Schneider, D. P. 1985, *AJ* 90, 1648.
- Huchra, J., Geller, M., Clemens, C., Tokarz, S. & Michel, A. 1995, *The CFA Redshift Catalogue*, Harvard-Smithsonian Center for Astrophysics, Cambridge, MA
- Kinney, A. L., Calzetti, D., Bohlin, R. C., McQuade, K., Storchi-Bergmann, T., and Schmitt, H. R. 1996 *apj* 467,38.
- Kriss, G. A. 1997, personal communication.
- Kurucz, R.L. 1992, in *The Stellar Populations of Galaxies*, ed. B. Barbuy & A. Renzini (Dordrecht: Kluwer Academic), 225.
- Landsman, W. B., Bohlin, R. C., O’Connell, R. W., Roberts, M. S., Smith, A. M., and Stecher, T.P. 1992 *ApJ* 401, L83.
- Lasker, B.M., Sturch, C.R., McLean, B.J., Russell, J.L., Jenkner, H. & Shara, M.M. 1989, *Space Telescope Science Institute Preprint No. 363*.
- Lequeux, J., Maucherat-Joubert, M., Deharveng, J. M., & Knuth, D. 1981, *A&A* 103, 305.
- Liu, C. T. & Green, R. F. 1996, *ApJ* 458, L63.
- Milliard, B., Donas, J., Laget, M., Armand, C., & Vuillemin, A., 1992, *A&A* 257, 24.
- Nilson, P. 1973, *Uppsala General Catalogue of Galaxies*, Uppsala Astron. Obs. Ann. Vol 6.
- Nordsieck, K., Code, A., Meade, M. *et al.* 1991 *BAAS* 23, 906.
- O’Connell, R. W. 1987 *AJ* 94, 876.
- Paturel, G., Fouque, P., Bottinelli, L., & Gouguenheim, L. 1989 *A&AS* 80, 299.
- Schaerer, D., Meynet, G., Maeder, A. & Schaller, G. 1992 *A&AS* 98, 523.
- Schaller, G., Schaerer, D., Meynet, G., and Maeder, A. 1992, *A&AS* 96, 269.
- Smith, E. P. personal communication.
- Stecher *et al.* 1992, *ApJ* 395, L1.
- Stecher, T. P., Cornett, R. H., Greason, M. R., Landsman, W. B., Hill, J. K., Hill, R. S., Bohlin, R. C., Chen, P. C., Collins, N. R., Fanelli, M. N., Hollis, J. I., Neff, S.G., O’Connell, R. W., Offenberg, J. D., Parise, R. A., Parker, J. Wm., Roberts, M. S., Smith, A. M., and Waller, W. H. 1997, *PASP* 109, 584.
- Struble, M. F. & Rood, H. J. 1987 *ApJS* 63, 543.
- Thompson, L. A. & Gregory, S. A. (1980) *ApJ* 242, 1.
- Valdes, F. 1982, *FOCAS User’s Manual*, Kitt Peak National Observatory, Computer Support Office, Tucson, AZ
- de Vaucouleurs, G., de Vaucouleurs, A., Corwin, H. G., Buta, R. J., Paturel, G., and Fouque, P. 1991, *Third Reference Catalogue of Bright Galaxies*, Springer-Verlag: New York Springer-Verlag: New York
- Veron-Cetty M. P. & Veron, P. 1996, *A Catalogue of Quasar and Active Nuclei*, 7th edition, E.S.O. Sci. Rep.

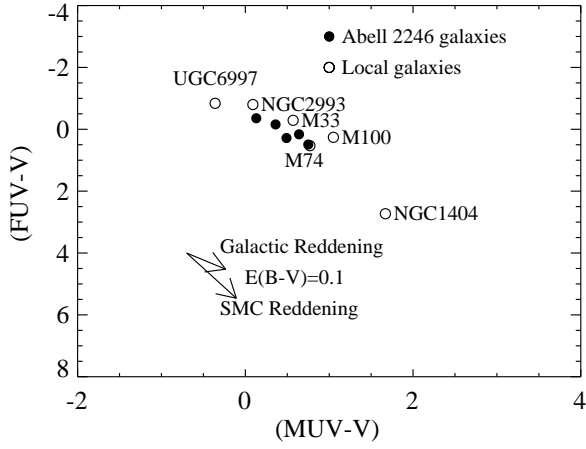


Fig. 4.— A comparison of the $(\text{MUV}-V, \text{FUV}-V)$ colors for Abell 2246 galaxies (filled circles) with those derived from total magnitudes of observed local galaxies (open circles, labelled). All objects are corrected for foreground extinction; the potential effect of internal “screen” reddening for $E(B-V)=0.1$ for Galactic and SMC extinction laws is shown by arrows. Abell 2246 galaxies observed at $z=0.225$ have slightly redder $\text{FUV}-V$ colors values than the rest-frame colors of the bluest star-forming systems that are plotted here.

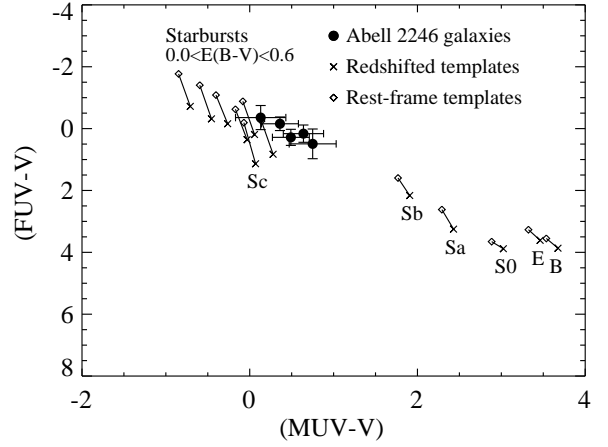


Fig. 5.— A comparison of the Abell 2246 data from Figure 4 with observation-based template galaxy spectra. Diamonds, from upper left to lower right, are the rest-frame colors of starbursts with small ($E(B-V) < 0.1$) to large ($E(B-V) \sim 0.5$) internal reddening, through galaxies of increasingly earlier (“Sc, Sb, Sa, S0, E”) type, to those of a bulge (“B”) population. Template colors are also plotted as redshifted to $z=0.225$ (crosses), connected to corresponding rest-frame template colors. Error bars shown here are appropriate for all color-color diagrams in this paper.

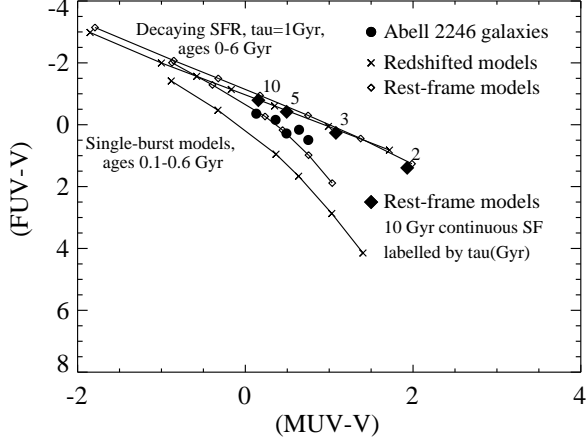


Fig. 6.— The observed MUV–V, FUV–V color-color data from Figure 4 displayed with the rest-frame (diamonds) and redshifted (crosses) evolutionary tracks of selected stellar population models. All models have IMF slopes -1.35 . The lower pair of model curves represent aging single-burst star formation, with ages ranging from age .1 Gyr (in the upper left of the diagram) to 0.6 Gyr (lower right) in ~ 0.1 Gyr increments. The upper pair of curves is a continuous-star-formation model, with a star formation rate which decreases exponentially with time constant $\tau=1$ Gyr, and ages from ~ 0 –6 Gyr in 1 Gyr increments. The observed galaxies show strong evidence of recent (<400 Myr) star formation. Both rest-frame and redshifted model colors are evenly spaced with time in (FUV–V), showing a simple power-law increase to redder color values. This reflects the exponential fall-off in numbers of the hottest stars (which dominate the FUV bandpass) caused by the decaying star formation rate; the strictly straight-line relationship of the redshifted model is caused by the bluer bandpass of observation which samples only extremely hot stars. The filled diamond symbols represent the rest-frame colors of models of 10-Gyr-old stellar populations with different SFR decay times, simulating a galaxy with a long history of star formation. After redshift correction, the best model for Abell 2246 galaxy colors evidently has star formation decay timescales of $3 \text{ Gyr} < \tau < 5 \text{ Gyr}$. This results in models which are ~ 0.5 mag too blue in (FUV–V); however, the single-burst model loci show that contributions from a single recent burst can add MUV and V flux without significant FUV.

This figure "a2fig1a.jpg" is available in "jpg" format from:

<http://arxiv.org/ps/astro-ph/9805111v1>

This figure "a2fig1b.jpg" is available in "jpg" format from:

<http://arxiv.org/ps/astro-ph/9805111v1>

This figure "a2fig1c.jpg" is available in "jpg" format from:

<http://arxiv.org/ps/astro-ph/9805111v1>

This figure "a2fig2.jpg" is available in "jpg" format from:

<http://arxiv.org/ps/astro-ph/9805111v1>